A 20 kW solid oxide electrolysis cell system with hydrogen recirculation: Operational performance and thermodynamic evaluation.

Anh Duc Nguyen[a, b], Jin Young Park[a], Yonggyun Bae[a, d], Dong Keun Lee[a], and Young Sang Kim[a,b,c]

[a] *Korea Institute of Machinery & Material, Daejeon, Republic of Korea, adn@kimm.re.kr CA*
[b] *University of Science and Technology, Daejeon, Republic of Korea*
[c] *School of Mechanical Engineering, Chung-Ang University, Seoul, Republic of Korea*
[d] *Chung-Ang University, Seoul, Republic of Korea*

Abstract

In response to the growing trend of verifying the performance of Solid Oxide Electrolysis Cell (SOEC) systems for commercialization, a 20 kW SOEC with a hydrogen recirculation system has been developed and analyzed. This marks the first comprehensive thermodynamic analysis of the operational results for a verified SOEC system. The experimental system consists of 4x5 kW-SOEC stacks, heat exchangers, one condenser, one air blower, one recirculation blower, four power supplies, and furnace heaters. Results show stable operation for over 3,000 hours, in two stages, with the stack temperature controlled at 730-750°C and steam conversion of 32-35%. The system electrical efficiency remains above 80% (41.4 kWh/kg H2), while the stacks themselves consume 35.92 kWh/kg H2. For further understanding, a comprehensive energy and exergy analysis is conducted to evaluate the heat loss and system irreversibility at two stages of the experiment. Energy analysis results show high thermal loss of unrecovered gas cooling latent heat, while the stack hot box follows as the 2nd major loss. In the second stage of the experiment, the thermal insulation of the hot boxes is enhanced, resulting in a 5.86% reduction in heat loss and a 1.42% increase in system efficiency. Exergy analysis reveals that system irreversibility occurs in SOEC stacks and furnace heaters, which account for 39.47% and 38.62% of the system exergy destruction ratio in Stage 2, respectively. The overall system exergy efficiency increases from 76.67% in Stage 1 to 78.03% in Stage 2, confirming that reducing heat loss from hot boxes improves system efficiency.

Keywords: Energy analysis; Exergy analysis; Hydrogen production; Solid oxide electrolysis cell; Solid oxide electrolysis cell system.

1. Introduction

Amid the escalating impacts of global warming, reducing greenhouse gas emissions has become an urgent global imperative. Global greenhouse gas emissions must peak by 2025 and subsequently decline to limit the increase in global mean temperature to 1.5 ^{o}C [1-3]. Strategic assessments have consistently projected that global hydrogen demand will increase exponentially in the coming decades [4]. Across decarbonization scenarios, hydrogen consumption is projected to account for approximately 2–10% of global final energy demand by 2050, substantially exceeding the current share of less than 2% [5]. Comparative analyses of major energy outlooks and industrial roadmaps indicate that hydrogen demand in 2050 will range from approximately 20 Mt to more than 300 Mt, with certain benchmark scenarios suggesting up to a sixteenfold increase relative to current levels [6]. Among the available hydrogen production pathways, water electrolysis is considered one of the most promising technologies, particularly when integrated with renewable energy sources [7]. Notably, Solid Oxide Electrolysis Cell (SOEC) technology exhibits the highest electrical efficiency among established electrolysis methods [8], particularly when coupled with high-temperature heat sources, such as nuclear power plants or industrial waste-heat recovery systems, which provide supplementary heat and steam [9, 10].

Validated SOEC systems have progressed from lab-scale to multi-megawatt installations. Gruber et al. at the Karlsruhe Institute of Technology demonstrated a pressurized SOEC–methanation system at 15 bar, achieving 90% steam conversion and 75–80% efficiency. High pressure reduced heater demand and improved efficiency. Sunfire showcased a 150 kW / 30 kW GrInHy rSOC system in a steel plant, operating for over 5,000 hours with around 84% electrolysis efficiency and low degradation rates (~21 $mW \cdot cm^{2} \cdot kh^{-1}$). [11, 12]. Additional work from DLR reported long-term operation of a 10 kW-class SOEC system with approximately 90% steam conversion, stable thermoneutral-level voltages, and a stack efficiency of 93% [13]. Subsequent analyses by Min quantified the system-level electrical efficiency as 59.2% [14]. Schwarze et al. documented

Sunfire's scale-up from 1–10 kW lab units to 150 kW systems and the 2.6 MW MULTIPLHY plant. They achieved power densities over 1 W/cm², reduced degradation to <1% per 1,000 hours, and reached system-level electrolysis efficiencies near 84% (LHV), indicating high readiness for MW-scale HTSE deployment. [15]. Jülich advanced a 5 kW SOFC/15 kW SOEC rSOC system, achieving 62–63% (LHV) in SOFC mode and around 70% (LHV) in SOEC mode over 9,000 hours, with low degradation (~0.6 mV kH^{-1}). The system scaled to 10 kW / 40 kW, reaching 63.3% (LHV) in SOFC mode and 71.1% (LHV) in SOEC mode, producing 11.7 Nm^3h^{-1} of H2 at 80% steam utilization. Loss analyses showed the steam-generation unit as the main SOEC inefficiency source [16, 17]. VTT conducted scaled rSOC demonstrations, starting with a 2 kW SOFC / 7 kW SOEC pilot unit that operated for over 2500 hours, achieving 81% AC-to-H2 efficiency and offering insights into multi-stack failure behavior. [18]. This work was followed by a movable 2 × 10 kW containerized rSOC system that achieved 71% HHV (81% HHV with external steam) and demonstrated scalability toward ≥100 kW modular installations [19]. The MULTIPLHY project showcased the first 2.6 MW SOEC plant in an industrial refinery, successfully passing factory acceptance testing with twelve Sunfire modules, producing ≥ 60 kg H_2/h at module efficiencies of 86% (LHV). [20]. Bloom Energy's 4 MW solid oxide electrolyzer system was successfully installed and operated at NASA's Ames Research Center [21]. These validation demonstrations show significant improvements in efficiency, thermal management, and modular scalability, marking the transition of SOEC technology from lab-scale to industrial MW-scale platforms.

Challenges persist in thermodynamically assessing SOEC systems despite positive outcomes. A systematic energy analysis is essential for evaluating their BOP components. Peters et al. analyzed energy losses in a 10/40 kW reversible solid oxide cell system at Forschungszentrum Jülich, achieving 71.1% efficiency, with major losses from steam generators and heating plates. [17]. Using a single energy metric to evaluate sustainable energy systems is often insufficient. Exergy analysis, which considers irreversible entropy generation, offers a more thorough framework for assessing efficiency and minimizing thermodynamic losses in sustainable energy technologies. [22]. Initial studies of solid oxide steam electrolysis found that exergy destruction primarily occurs in the SOEC stack, rather than in heat exchangers as previously thought. Optimizing stack temperature, current density, and steam conversion improved both energy and exergy efficiencies, with better thermal management at higher temperatures. [23]. Müller and Tsatsaronis analyzed exergy in pressurized and near-atmospheric SOEC systems, finding that the stack was the main source of exergy destruction, followed by heat exchangers. The system's exergetic efficiency improves with higher inlet steam ratios and optimized temperatures, but excessive current density increases exergy destruction in the stack. [24]. As discussed, exergy analysis facilitates the identification of the magnitudes and sources of thermodynamic inefficiencies [25]. These insights help develop strategies to improve the thermodynamic performance of systems. However, most parametric analyses are theoretical, and there is a notable lack of comprehensive exergy analyses using real operational data, which are crucial for interpreting experimental results. [26].

This study analyzes operational data from a validated 20 kW Solid Oxide Electrolysis Cell (SOEC) system with hydrogen recirculation, operated for over 3,000 hours in two stages. The key objective was to enhance system efficiency through exergetic analysis. Initially, experimental data is adapted to calculate enthalpy and heat generation. Next, energy analysis quantified system heat losses, followed by exergy analysis to identify thermodynamic irreversibility sources. This comprehensive approach aims to support the design optimization and scale-up of high-temperature electrolysis technologies.

2. System description and experiment

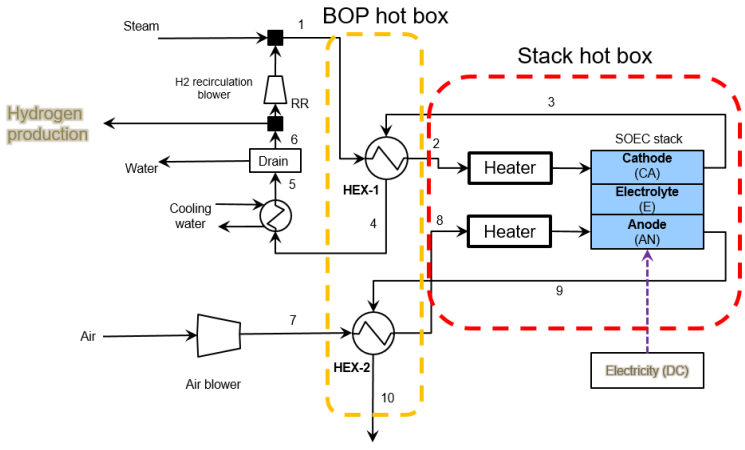

Figure. 1. *Schematic of the experimented 20kW SOEC with recirculation system*

Figure 1 shows a schematic of the 20 kW SOEC system, which includes a thermally integrated SOEC stack hot box and a balance-of-plant (BOP) hot box. It also features two heat exchangers, manifolds, and a blower-based hydrogen recirculation system for safe operation without an external hydrogen tank.

The feed steam is evaporated and mixed with a recycled hydrogen-rich stream, forming a steam–H_2 mixture that enters the BOP hot box. Here, it undergoes heat recovery in Heat Exchanger 1 and is heated to the SOEC stacks' operating temperature. In the SOEC stack, hydrogen is produced via electrolysis, with the hot outlet mixture transferring thermal energy back to the inlet streams through Heat Exchanger 1. This stream is cooled using a condenser to remove water, and the processed H_2 is split: part is used as the hydrogen product stream, while the rest is recirculated to maintain a 9:1 Steam–H_2 ratio.

An air blower supplies air to the air electrode, which is preheated by Heat Exchanger 2 using heat from the cathode off-gas before entering the SOEC stack anode. Heat from the anode off-gas is also recovered in Heat Exchanger 2 before venting. Two furnace heaters in the stack hot box control temperature and preheat the inlet air and fuel streams.

Fig. 2(a) shows the experimental setup of the SOEC system, while Fig. 2(b) highlights the SOEC stack hot box and the BOP hot box. The experiment utilized four 5 kW planar fuel-electrode-supported SOEC stacks. Temperature sensors were placed at the inlet and outlet of each stack for air and fuel flows, and pressure sensors were positioned near the flanges in the air and fuel pipes.

The tests were conducted for more than 3,000 h. The fuel utilization of the stacks was maintained at a relatively low level, between 32% and 36%, to ensure mild operating conditions. During system start-up, the stack hot box reached the target temperature of 740 °C within 50 h. During this process, the stacks received 5 L min^{-1} of hydrogen, 55 L min^{-1} of nitrogen, and an air flow rate of 193 L min^{-1}.

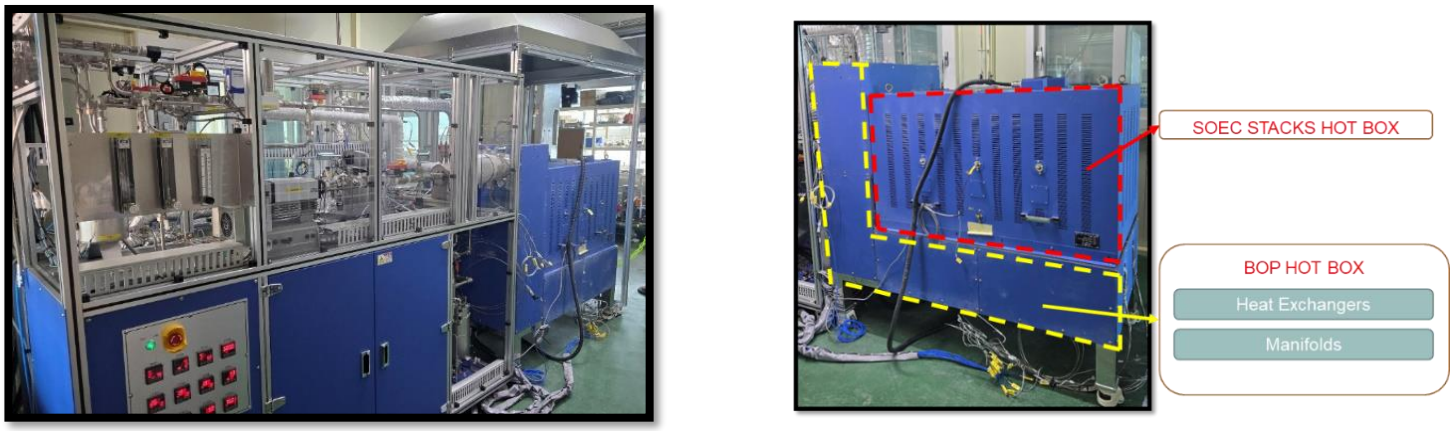

(a) (b)

Figure. 2. *(a) System experiment set up, (b) Stack hot box and BOP hot box.*

After the temperature ramp-up, the stack was maintained in hot-standby mode for 68 h until thermal equilibrium was reached. During this period, hydrogen was supplied at a rate of 35 L min^{-1}, nitrogen supply was discontinued, and the air flow rate was gradually reduced to 80 L min^{-1}. The electrolysis phase began after this stage. During electrolysis, water was supplied at a rate of 210 cm^3 min^{-1} to generate steam, and the current density was gradually increased from zero to the desired level over 160 min.

The stack operated stably with a water supply of 240 cm^3 min^{-1} delivered through four steam generators and 30 L min^{-1} of hydrogen. Hydrogen serves as a protective gas to prevent the oxidation of nickel–yttria-stabilized zirconia (YSZ) fuel electrodes to nickel oxide (NiO) and YSZ [27].

3. Methodology

3.1. System energy analysis

The overall system was modeled, and its performance was analyzed using the commercial Software EBSILON® Professional [28]. In addition to the SOEC stack, other BOP components were modeled using a built-in software library with adjusted parameters to match the experimentally recorded power consumption and thermal conditions. The software takes input data on the measured temperature, pressure, flow rate, and power consumption and subsequently calculates the relevant enthalpy values. Using these enthalpy calculations, the heat losses from the SOEC stack, BOP components, and piping were estimated. The energy and enthalpy balances are expressed using Eq. (1), where $\dot{m}$ and h represent the mass flow rate and specific enthalpy of the ith and jth streams, respectively.

$$\Delta H = \left(\sum_{i=1}^{n} \dot{m}_i h_i\right)_{incomingstream} - \left(\sum_{j=1}^{m} \dot{m}_j h_j\right)_{outgoingstream} \quad (1)$$

For the overall system, the energy balance was determined using Eq. (2), where m, LHV, Q, and W represent the mass flow rate, lower heating value, heat transfer, and electricity power, respectively.

$$\dot{W_{SOEC}} + \dot{W_{BOP}} = (\dot{m}\mathrm{LHV})_{\mathrm{H_2},produced} + \dot{Q_{Loss}} \quad (2)$$

The total system electrical efficiency is calculated using Eq. 3:

$$\varepsilon_{tot} = \frac{(\dot{m}\mathrm{LHV})_{\mathrm{H_2},produced}}{\dot{W_{SOEC}} + \dot{W_{BOP}}} \quad (3)$$

3.2. System exergetic analysis

Energy analysis quantifies the energy flow of each component and the overall system, revealing that heat loss and inefficient energy utilization reduce overall system efficiency. However, energy analysis alone cannot provide quantitative information regarding thermodynamic inefficiencies [29]. In exergy analysis, the total exergy $\dot{E}_i$ of a material stream i consisting of chemical species j is expressed as the sum of the physical and chemical exergies [25].

$$\dot{E}_{total} = \dot{E}^{PH} + \dot{E}^{CH} = \dot{m}(e^{PH} + e^{CH}) \quad (4)$$

The physical exergy (e^{PH}), which is associated with the temperature and pressure of the system, was calculated using Eq. (5). Whereh_0,T_0,$s_0$represent the enthalpy, temperature, and entropy of the restricted dead state [29], h, and s are the tabulated enthalpy and entropy values of the corresponding stream obtained using Cantera [30].

$$e^{PH} = (h - h_0) - T_0(s - s_0) \quad (5)$$

The chemical exergy $(e^{CH})$is obtained from the difference between the chemical compositions of the analyzed state and the thermodynamic environment [31]. In this study, the gas mixture was assumed to be ideal. Eq. 6 was used to calculate the chemical exergy of the ideal gas mixture using the molar composition (x_i) and the standard chemical exergy of each component (e_i^{CH}), which was obtained from [32].

$$e^{CH}_{idealgasmixture} = \sum_{i=1}^{N} x_i e_i^{CH} + \bar{R}T_0 \sum_{i=1}^{N} x_i \ln(x_i) \quad (6)$$

In an exergetic analysis, the exergy of the fuel and the product of each component should be defined. For components involving chemical reactions, the chemical and physical exergies are considered separately to enable precise analysis [33]. The exergy of the product generated by a component or system is defined as the desired output and expressed in exergy units. The exergy of the fuel represents the exergetic resources required to generate the exergy of the product. Table 1 summarizes the definitions of the exergy terms for both the fuel and the product of each component. For the SOEC stack, the increased sensible energy on the anode and cathode sides enhances the physical exergy component of the product exergy because it helps maintain the thermal integrity of downstream components.

Table 1. *Definition of the exergy of fuel and product of selected components.*

Component	Exergy of fuel (kW)	Exergy of product (kW)
SOEC	$\dot{W}^{PH}_{electrical}$	$(\dot{E}^{CH}_{Ca\,out} - \dot{E}^{CH}_{Ca\,in}) + (\dot{E}^{CH}_{An\,out} - \dot{E}^{CH}_{An\,in}) + (\dot{E}^{PH}_{Ca\,out} - \dot{E}^{PH}_{Ca\,in}) + (\dot{E}^{PH}_{An\,out} - \dot{E}^{PH}_{An\,in})$
Air Blower	$\dot{W}_{electrical}$	$(\dot{E}^{PH}_{out} - \dot{E}^{PH}_{in})$
RC Blower	$\dot{W}_{electrical}$	$(\dot{E}^{PH}_{out} - \dot{E}^{PH}_{in})$
Fuel HEX	$(\dot{E}^{PH}_{hot,in} - \dot{E}^{PH}_{hot,out})$	$(\dot{E}^{PH}_{cold,out} - \dot{E}^{PH}_{cold,in})$
Air HEX	$(\dot{E}^{PH}_{hot,in} - \dot{E}^{PH}_{hot,out})$	$(\dot{E}^{PH}_{cold,out} - \dot{E}^{PH}_{cold,in})$
Mixer	$\dot{E}_{in,1} + \dot{E}_{in,2}$	$\dot{E}_{out}$
Heater	$\dot{W}_{electrical}$	$(\dot{E}^{PH}_{a,in} - \dot{E}^{PH}_{8})$+$(\dot{E}^{PH}_{f,in} - \dot{E}^{PH}_{2})$
Pipe	$\dot{E}_{in}$	$\dot{E}_{out}$

The exergetic efficiency (ε_k) is defined as the ratio of the exergy of the product to the exergy of the fuel. This metric represents the thermodynamic performance of the analyzed components within the overall system.

$$\varepsilon_k = \dot{E}_{P,k}/\dot{E}_{F,k} \quad (7)$$

The exergy destruction ratio (y_k^*) of each component is defined as the ratio of the exergy destruction within that component to the total exergy destruction of the entire system. This value can be used as an indicator of potential thermodynamic improvement.

$$y_k^* = \frac{\dot{E}_{D,k}}{\sum_{k=1}^{N} \dot{E}_{D,k}} \quad (8)$$

Finally, the exergy efficiency of the entire system was calculated as follows: The exergetic efficiency of an overall process is defined as the ratio of the exergetic product to the exergetic fuel.` The exergetic product can also be expressed as the difference between fuel exergy, exergy loss, and exergy destruction [9].

$$\varepsilon_{tot} = \frac{\dot{E}_{P,tot}}{\dot{E}_{F,tot}} = \frac{\dot{E}_{F,tot} - \left(\dot{E}_{D,tot} + \dot{E}_{L,tot}\right)}{\dot{E}_{F,tot}} \quad (23)$$

4. SOEC system analysis results

4.1. SOEC system long-term operation result:

Table 2. *Operating conditions of the SOEC stacks in two stages*

Operating parameter	Stage I	Stage II	
Stack temperature ($\boldsymbol{T}$)	730	750	°C
Stack outlet temperature ($\boldsymbol{T_{out}}$)	785	768.5	°C
Steam utilization ($\boldsymbol{FU}$)	0.355	0.32	-
Molar fraction of Hydrogen inlet ($\boldsymbol{X_{H2}}$)	0.1	0.1	-
Average cell current density($\boldsymbol{J}$)	6540	6446.5	A/m^2
Average cell voltage ($\boldsymbol{U_{cell}}$)	1.301	1.285	V

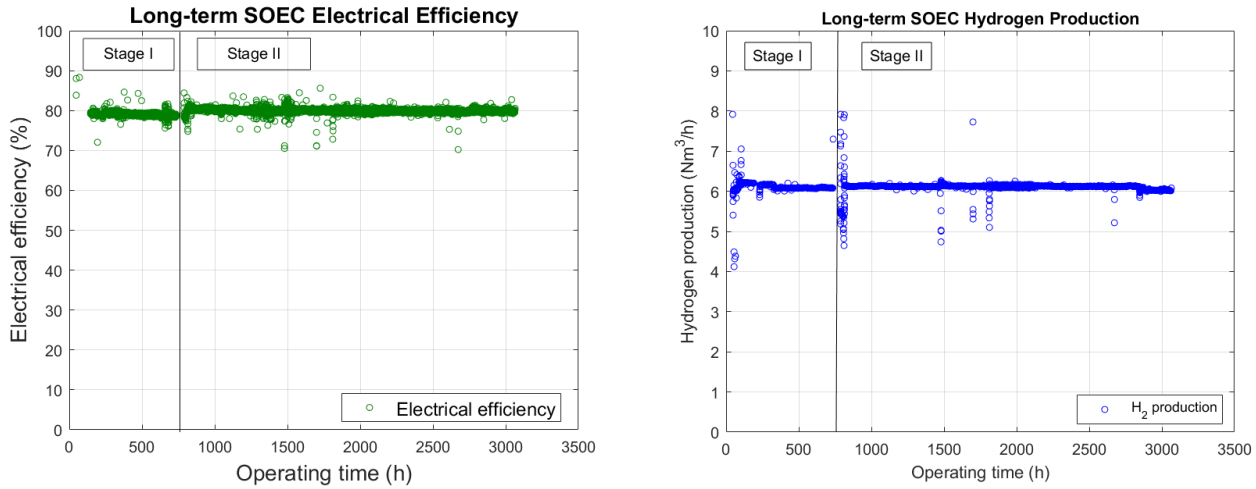

(a) **(b)**

Figure. 3. *Long-term operation of the SOEC system (a) System efficiency (%), (b) System hydrogen production rate*

Figures 3(a) and 3(b) summarize the long-term operational performance of the 20 kW-class SOEC system, highlighting two distinct operating stages separated by an unplanned shutdown event. During Stage I, corresponding to the initial system configuration, the SOEC operated stably at a hydrogen production rate of approximately 6–6.3 Nm³ h^{-1}, with the system efficiency predominantly in the 78–79% range, although noticeable fluctuations and occasional drops to approximately 75% were observed. Stage I corresponds to the initial system configuration in which the SOEC operated without thermal insulation in the manifold region. This stage ended with an unplanned system shutdown due to an external power outage, which interrupted the steam supply and led to irreversible stack degradation. Following this shutdown, the degraded stack was replaced with an identical unit, and the thermal insulation of the system was improved. In Stage II, additional insulation layers were applied not only to the manifold region but also to other hot BOP components, after which the system was returned to operation. During this stage, the stacks were operated at a lower steam utilization rate of 32% compared with 35% in Stage I. This milder operating condition was implemented to achieve the target of 3,000 h. The operating conditions of the SOEC stack during two stages are summarized in Table 2. As shown in Fig. 3, Stage II exhibited a clear upward shift and narrowing of the efficiency distribution, stabilizing at 80–81%, while maintaining a comparable hydrogen production rate of approximately 6.2 Nm^{3}h^{-1}. The improved efficiency in Stage II was primarily attributed to reduced parasitic heater demand and enhanced internal heat recovery within the stack hot box, enabled by lower thermal losses to the environment. Therefore, the midpoint transition indicated in Fig. 3(a) represent not only hardware replacement but also system-level thermal improvement, demonstrating that insulation quality and heat management play a decisive role in sustaining high-efficiency SOEC operation at comparable hydrogen production rates. Detailed thermal balance, energy, and exergy analyses are presented in the following sections.

4.2. System energy analysis result

Figure 4 shows heat flow distributions in the stack and BOP hot boxes during two operating stages. The diagrams quantify contributions from process gas enthalpy, electrical heating, internally generated stack heat, and thermal losses. This allows for a direct comparison of thermal behavior before and after system refurbishment.

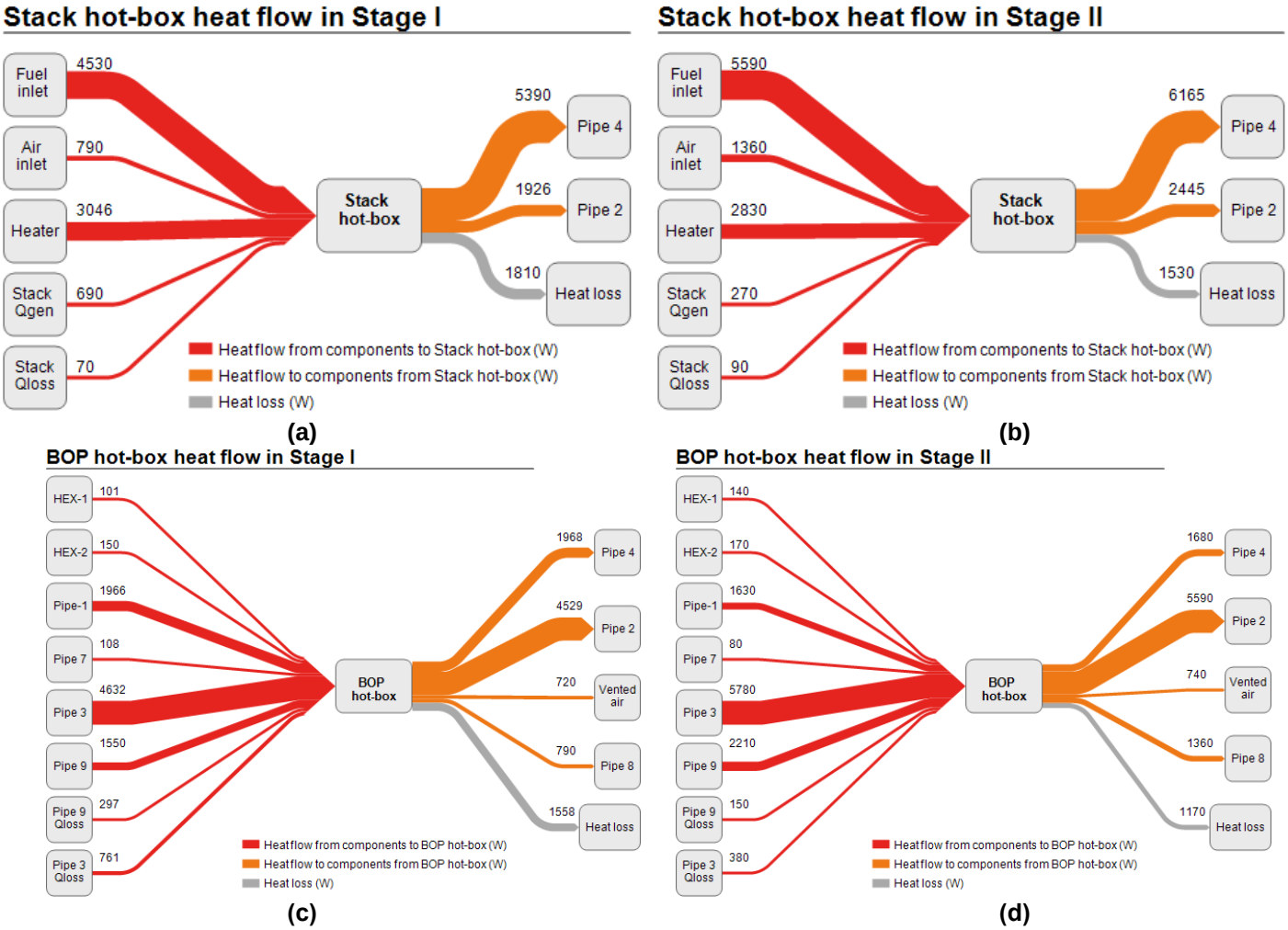

Figure. 4. *System heat flow of the (a) Stack hot box of Stage I, (b) Stack hot box of Stage II, (c) BOP hot box of Stage I, and (d) BOP hot box of Stage II*

This section focuses on the stack hot box and BOP hot box as control volumes. The model computes heat generated by the stacks, which raises the temperature of fuel and air streams. Hot outlet streams transfer heat to the internal space of hot box, calculated from the difference between theoretical and measured outlet temperatures. The electrical heaters are based on the power consumption of two furnace heaters supplying heat to the inlet streams and compensating for heat losses. Pipes 4 and 2 represent the fuel and air streams exiting the hot box.

The stack hot box has a total incoming heat flow of about 9.13 kW, primarily from the fuel inlet stream (4.53 kW) and furnace heating (3.05 kW), along with smaller contributions from air inlet enthalpy (0.79 kW) and stack-generated heat (0.69 kW). The outlet streams carry away most thermal energy (5.39 kW for fuel and 1.92 kW for air), but 1.81 kW is lost to the surroundings, indicating poor insulation. This section analyzes the stack and BOP hot boxes to evaluate heat generation and transfer efficiency.

After improvements in Stage II, total heat flow increases to 10.14 kW, while furnace heating power drops to 2.83 kW, reflecting reduced heat loss. Stack-generated heat decreases to 0.27 kW, nearing thermoneutral operation, and environmental heat loss falls to 1.53 kW. This enhances system efficiency by allowing more thermal energy to increase outlet gas enthalpy. The outlet thermal energy is primarily carried by fuel and air outlet streams (5.39 kW and 1.92 kW), with 1.81 kW still lost to the surroundings, indicating inadequate insulation in Stage I. With insulation improvements after stack replacement, Stage II shows a better thermal balance.

For the BOP hot box, Stage I shows a total heat entry of 9.66 kW, primarily from heated streams (Pipe 2 and Pipe 3 contributing 4.53 kW and 4.63 kW), but cumulative heat loss to the environment is 1.54 kW, plus additional losses from pipelines (~1.06 kW). This indicates that a substantial amount of recovered heat from upstream components is lost, diminishing the benefits of heat integration.

The BOP hot box heat throughput increases to 10.54 kW due to higher pipeline stream enthalpy, while environmental heat loss decreases to 1.17 kW, a 24% reduction from Stage I. Reduced losses in major lines like Pipes 1 and 9 indicate improved thermal retention, enhancing hot-box performance. Upgrades from Stage I to II have minimized thermal losses in both the stack and BOP hot boxes, lowering heating demand and environmental heat loss, thus improving system efficiency while maintaining consistent hydrogen production. Effective thermal insulation and heat management are crucial for medium- and large-scale SOEC systems, as they reduce heat rejection, lower auxiliary power consumption, and stabilize stack inlet conditions for better durability and robustness.

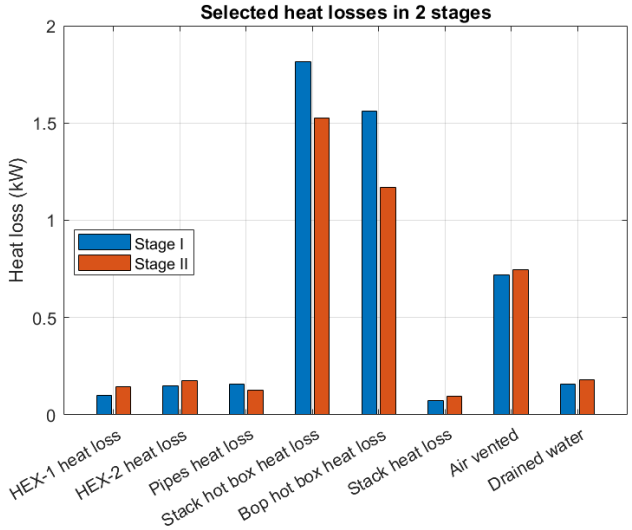

Figure. 5. *Comparison of selected heat losses in Stage I and Stage II.*

Figure 5 compares heat losses in both stages, highlighting that hot boxes are the primary sources of loss. In Stage I, the stack hot box (≈1.8 kW) and BOP hot box (≈1.6 kW) have the largest losses due to heat leakage. Improvements in Stage II reduce these losses (stack hot box to ≈1.5 kW and BOP hot box to ≈1.2 kW). Pipeline heat loss decreases slightly, while losses from HEX-1/HEX-2 remain low (<0.2 kW) and may increase with higher system temperatures. Further improvements are needed to reduce vent flows and recover latent heat from exhaust.

Figure 6 shows the heat balance of the 20 kW SOEC system during (a) Stage I and (b) Stage II operations, detailing electrical power consumption, reactant enthalpy, auxiliary heating, and thermal losses. The primary energy input is electrical power to the SOEC stack (19.06 kW in Stage I and 18.55 kW in Stage II), followed by inlet steam's enthalpy (10.85 kW and 11.28 kW, respectively). Auxiliary heating decreases slightly from 3.05 kW in Stage I to 2.83 kW in Stage II due to improved thermal insulation and heat recovery.

The useful energy output, represented by the lower heating value (LHV) of the produced hydrogen, remains comparable between the two stages (17.45 kW in Stage I and 17.20 kW in Stage II). The remaining energy is distributed among several loss pathways, including stack hot-box heat loss (1.81 to 1.53 kW), BOP hot-box heat loss (1.54 to 1.17 kW), pipe heat losses (0.06 to 0.13 kW), and controlled heat rejection via gas cooling (7.70 to 8.17 kW).

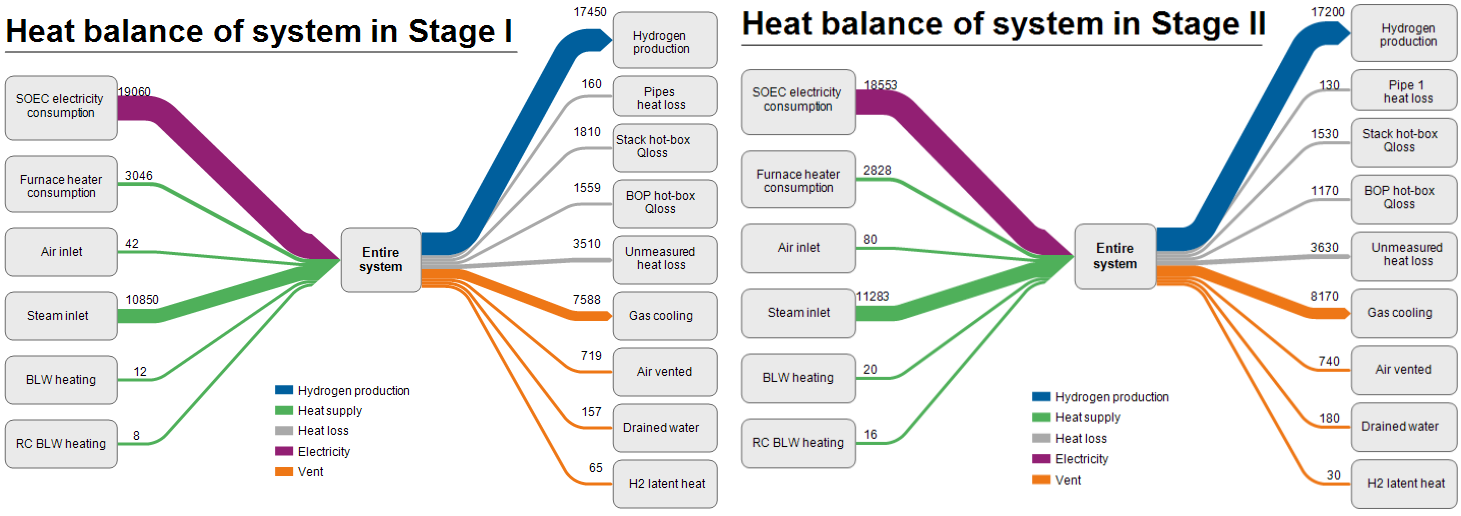

Figure. 6. *Overall heat balance of the entire system (a) Stage I, and (b) Stage II*

In stage II, the stacks operated at a lower current density, improving efficiency to 92.7% from 91.55% in stage I. However, this increase had limited overall impact due to higher inlet steam energy and cooling requirements. The main enhancement stemmed from better thermal insulation, which reduced passive heat losses from 3.35 kW in stage I to 2.70 kW in stage II, a 19% decrease. This reduction lowered auxiliary heating demands and improved heat utilization, leading to less furnace power needed and more stable thermal operation. Additionally, increased heat rejection via gas cooling in stage II helped manage temperature and maintain favorable thermal gradients.

Despite the detailed accounting of major heat flows, there remains an unmeasured loss term of 3.54 kW in Stage I and 3.63 kW in Stage II. This term accounts for distributed thermal loss processes that cannot be quantified experimentally, such as radiative losses from unmeasured surfaces, heat transfer through the system frame, and minor convective losses. The consistent value of these losses between the two stages confirms that the observed efficiency gain is a genuine result of reduced, directly measured environmental heat losses, rather than an artifact of heat-balance accounting.

The system-level heat balance showed that the efficiency gains in Stage II were mainly due to better thermal containment, not changes in electrochemical conversion or hydrogen production rates. Reduced furnace heating demand and lower hot-box heat losses allow more electrical energy to be converted into useful hydrogen. These results highlight the importance of optimizing insulation and heat flow pathways for high-efficiency operation in medium-scale SOEC systems.

4.3. System exergy analysis result

***Table 3**. Exergetic analysis of selected BOP in Stage I*

Component	Exergy of fuel - kW	Exergy of product - kW	Destruction - kW	Exergy efficiency (ε) - %	Destruction ratio (yk*) - %
SOEC	19.062	16.891	2.171	88.610	36.190
Air blower	0.073	0.003	0.070	3.646	1.166
Recirculation blower	0.022	0.010	0.012	44.455	0.208
Fuel HEX	1.483	1.314	0.169	88.629	2.810
Air HEX	0.481	0.318	0.163	66.172	2.713
Mixer	7.900	7.696	0.204	97.420	3.397
Stack hot box Heater	3.046	0.588	2.458	19.293	40.975
Piping	11.437	10.684	0.752	93.421	12.542

***Table 4**.Exergetic analysis of selected BOP in Stage II*

Component	Exergy of fuel - kW	Exergy of product - kW	Destruction - kW	Exergy efficiency (ε) - %	Destruction ratio (yk*) - %
SOEC	18.553	16.331	2.222	88.021	39.472
Air blower	0.092	0.007	0.085	7.774	1.502
Recirculation blower	0.032	0.013	0.019	40.397	0.339
Fuel HEX	2.357	2.102	0.255	89.191	4.525
Air HEX	0.849	0.613	0.236	72.195	4.193
Mixer	8.389	8.184	0.205	97.560	3.636
Stack hot box Heater	2.828	0.653	2.175	23.103	38.623
Piping	13.216	12.782	0.434	96.715	7.710

The exergetic performances of the SOEC system components are summarized in Tables 3 and 4. The SOEC stack was the primary source of irreversibility, contributing 36.19% and 39.472% of total exergy destruction in the two stages, respectively, due to electrochemical overpotentials and ohmic losses. It maintained high exergetic efficiencies of 88.6% (Stage 1) and 88.0% (Stage 2), effectively converting inlet exergy into chemical

and physical exergy of the outlet streams. The heater was the second-largest contributor to exergy destruction, accounting for 41.0% and 38.6% in the two stages. Improvements in Stage II raised total BOP exergy efficiency from 86.2% to 87.8% by reducing piping irreversibility and enhancing the efficiencies of the fuel and air heat exchangers. In contrast, rotating equipment like blowers exhibited low exergetic efficiencies (<10%). Overall, while the electrochemical stack limits performance, improvements in thermal management can enhance exergetic efficiency.

The SOEC stack exhibited a slightly higher exergy efficiency in Stage I than in Stage II when the product exergy was defined as the increase in the total exergy of the fuel and air streams across the stack, and the input exergy was the electrical power. As presented in Table 2, although Stage I operates at a marginally higher average cell voltage (1.301 V vs 1.285 V), which increases the electrical exergy input, it also shows a much larger exhaust temperature rise (from 730 °C to 785 °C) than Stage II (from 750 °C to 768.5 °C). This higher outlet temperature directly increases the physical exergy of both outlet streams, contributing positively to the system exergy efficiency. In addition, Stage I achieved a higher steam utilization (0.355 vs. 0.32) at a similar inlet fuel composition (X_{H2} = 0.1), implying less product dilution by residual steam and therefore a slightly higher chemical exergy gain in the outlet fuel stream. The average current density was comparable between the two stages (0.654 vs. 0.645 A.cm^{-2}); therefore, the observed exergy efficiency difference was primarily attributed to the combined effects of (i) the larger sensible-heat recovery potential reflected by the higher. T_{out} in Stage I, and (ii) higher conversion (FU), which together outweigh the penalty of a slightly higher operating voltage.

Table 5. *System exergy efficiency during Stage I and Stage II operation*

	Exergy of fuel - kW	Exergy of product - kW	Exergy loss/destruction - kW	System exergy efficiency - %
Stage I	22.20	17.02	5.18	76.67
Stage II	21.50	16.78	4.72	78.03

Table 5 compares the exergetic performance of the SOEC system in Stages I and II. The fuel exergy decreases from 22.20 kW in Stage I to 21.50 kW in Stage II, while the product exergy of hydrogen production remains nearly unchanged (17.02 kW and 16.78 kW, respectively). Consequently, the overall system exergy efficiency improved from 76.67% to 78.03% in Stage II, highlighting more effective conversion of electrical exergy to hydrogen's chemical exergy due to better thermal insulation and reduced auxiliary power demand, rather than changes in the electrochemical characteristics of the stack. Additionally, fuel exergy excludes the exergy of inlet steam, as the thermal energy for steam generation can come from an external waste-heat source, typical in thermally integrated SOEC systems. [34, 35]. When the inlet steam is included in fuel exergy, the exergy efficiencies for Stages I and II are 68.74% and 69.73%, respectively.

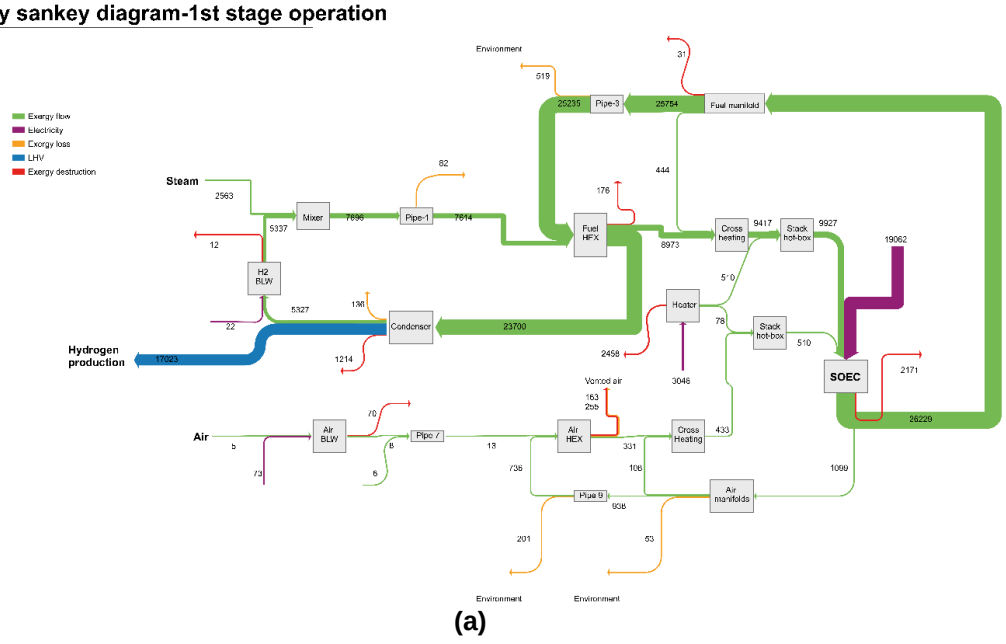

(a)

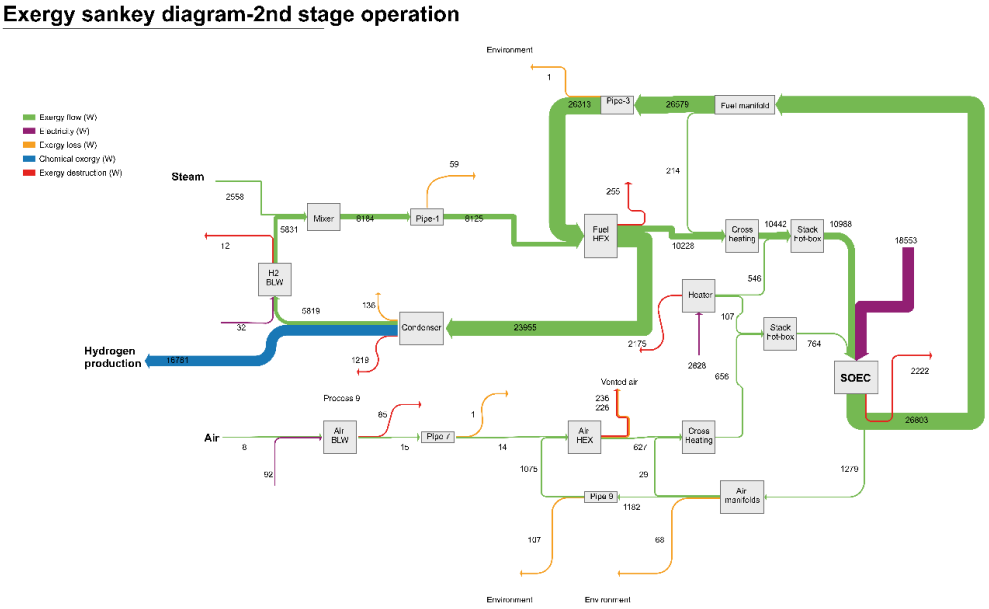

(b)

Figure. 7. *Exergy flow of the entire system in (a) Stage I, and (b) Stage II*

Figure 7(a–b) compares the exergy pathways of the integrated SOEC stack and hot-box BOP during two operating stages, emphasizing where irreversibilities occur. The primary exergy supply remains the electrical input to the stack (19.06 kW in Stage I vs 18.55 kW in Stage II), with minor contributions from the heaters and blowers. The useful output, chemical exergy of hydrogen, is similar in both stages (17.02 kW in Stage I and 16.78 kW in Stage II), indicating consistent production rates. The largest exergy destruction is in the SOEC stack (2.17–2.22 kW) and the heater (2.46 kW in Stage I, reduced to 2.18 kW in Stage II), followed by the condenser (1.21 kW in both stages). Direct exergy losses to the environment are smaller, mainly from the hot piping and vent streams, with a notable reduction from Pipe-3 in Stage II. The findings suggest that future improvements should focus on minimizing irreversibility in the stack and heater, recovering condenser heat for feed water preheating, and optimizing vent flows to reduce exergy losses.

5. Conclusion

This paper evaluates a 20 kW solid oxide electrolysis cell (SOEC) system with hydrogen recirculation, based on over 3,000 hours of validated operation. It includes an energy and exergy analysis to assess heat flows and identify irreversibility sources. Results show that performance improvement after refurbishment is due to better thermal management, specifically reduced heat losses in the hot box, rather than electrochemical changes. This underscores the importance of effective thermal integration and insulation quality for medium-scale SOEC efficiency.

The SOEC system operated stably for over 3,000 hours, producing approximately 6.2 $Nm^3 \cdot h^{-1}$ of hydrogen. In Stage I, the efficiency was about 79%, limited by thermal losses. After stack replacement and insulation upgrades in Stage II, efficiency improved to 80%, maintaining the same hydrogen output and demonstrating the benefits of refurbishment. Key thermal losses included unrecovered gas-cooling heat and losses from hot boxes, which increased electrical heating demand in Stage I. However, insulation upgrades in Stage II achieved a 19% reduction in heat losses, reducing heater power consumption. An unmeasured residual heat-loss term indicated genuine improvements in heat loss, independent of measurement uncertainty. Exergy analysis revealed that the SOEC stack and electric heaters were responsible for over 75% of total exergy destruction. Despite significant irreversibilities, the stack achieved an exergetic efficiency of about 88%. Overall system exergy efficiency improved from 76.67% in Stage I to 78.03% in Stage II, primarily due to reduced thermal irreversibility. To sum up, effective thermal management is crucial for SOEC efficiency. As power capacity increases, optimizing insulation, enhancing heat integration, and reducing auxiliary power consumption will be essential for minimizing thermal losses and improving thermodynamic performance. Continuous improvements at the stack level are also necessary to reduce electrochemical irreversibility.

Nomenclature

Greek Symbols

γ	Pre-exponential factor of the fuel electrode
η	Efficiency, [%]
ϵ	Exergy efficiency, %

Roman Symbols

E	Exergy (total, physical PH, or chemical CH), kW
e	Specific exergy, kJ/kg

LHV	Lower heating value, kJ/kg
$\dot{m}$	Mass flow rate, kg/s
n, m	Exponent factor of the anode/cathode exchange current density
P	Pressure, bar
s	Specific entropy, kJ/kg.K
T	Temperature, °C
U	Voltage, V
W	Electrical power / Work, kW
y_k^*	Exergy destruction ratio

Subscript

o	Reference (dead) state / Standard state
D	Destruction
F/P	Fuel/Product
tot	Total

Abbreviation

BOP	Balance of Plant
HHV	Higher Heating Value
HTSE	High-Temperature Steam Electrolysis
LHV	Lower Heating Value
RSOC	Reversible Solid Oxide Cell
SOEC	Solid Oxide Electrolysis Cell

Acknowledgments

This research was supported by the program of H2 Next Round through the National Research Foundation of Korea (NRF) funded by the Ministry of Science and ICT (RS-2024-00467191). And this work was also supported by the Korea Institute of Energy Technology Evaluation and Planning (KETEP) and the Ministry of Trade, Industry & Energy (MOTIE) of the Republic of Korea (RS-2025-16066396).

REFERENCES

[1] Riahi K, Schaeffer R, Arango J, Calvin K, Guivarch C, Hasegawa T, et al. Mitigation Pathways Compatible with Long-term Goals (Chapter 3). IPCC 2022: Climate Change 2022: Mitigation of Climate Change Contribution of Working Group III to the Sixth Assessment Report of the Intergovernmental Panel on Climate Change 2023:295–408.

[2] IEA. Net Zero Roadmap: A Global Pathway to Keep the 1.5 °C Goal in Reach. 2023.

[3] Kikstra JS, Nicholls ZR, Smith CJ, Lewis J, Lamboll RD, Byers E, et al. The IPCC Sixth Assessment Report WGIII climate assessment of mitigation pathways: from emissions to global temperatures. Geoscientific Model Development 2022;15(24):9075–9109.

[4] IEA. Global Hydrogen Review 2023. 2023.

[5] Terlouw T, Rosa L, Bauer C, McKenna R. Future hydrogen economies imply environmental trade-offs and a supply-demand mismatch. Nat Commun 2024;15(1):7043.

[6] Abid H, Østergaard PA, Skov IR, Mathiesen BV. Comparative assessment of future hydrogen demand potentials in a decarbonised European energy system. International Journal of Hydrogen Energy 2025;122:82–96.

[7] Dickson R, Abbas A, Lee Y, Liu J, Niaz H. A global perspective on solar-driven hydrogen economy and 2050 carbon neutrality. Chemical Engineering Journal 2025:164144.

[8] Sanz-Bermejo J, Gallardo-Natividad V, González-Aguilar J, Romero M. Coupling of a solid-oxide cell unit and a linear fresnel reflector field for grid management. Energy Procedia 2014;57:706–715.

[9] Zhao Y, Xue H, Jin X, Xiong B, Liu R, Peng Y, et al. System level heat integration and efficiency analysis of hydrogen production process based on solid oxide electrolysis cells. International Journal of Hydrogen Energy 2021;46(77):38163–38174.

[10] Yoon KJ, Lee S, Park S-Y, Minh NQ. Advances in high-temperature solid oxide electrolysis technology for clean hydrogen and chemical production: materials, cells, stacks, systems and economics. Progress in Materials Science 2025;154.
[11] Schwarze K, Posdziech O, Mermelstein J, Kroop S. Operational Results of an 150/30 kW RSOC System in an Industrial Environment. Fuel Cells 2019;19(4):374–380.
[12] Posdziech O, Schwarze K, Brabandt J. Efficient hydrogen production for industry and electricity storage via high-temperature electrolysis. International Journal of Hydrogen Energy 2019;44(35):19089–19101.
[13] Schiller G, Lang M, Szabo P, Monnerie N, von Storch H, Reinhold J, et al. Solar heat integrated solid oxide steam electrolysis for highly efficient hydrogen production. Journal of power sources 2019;416:72–78.
[14] Min G, Choi S, Hong J. A review of solid oxide steam-electrolysis cell systems: Thermodynamics and thermal integration. Applied Energy 2022;328.
[15] Schwarze K, Geißler T, Nimtz M, Blumentritt R. Demonstration and scale-up of high-temperature electrolysis systems. Fuel Cells 2023;23(6):492–500.
[16] Peters R, Frank M, Tiedemann W, Hoven I, Deja R, Kruse N, et al. Long-term experience with a 5/15kW-class reversible solid oxide cell system. Journal of the Electrochemical Society 2021;168(1):014508.
[17] Peters R, Tiedemann W, Hoven I, Deja R, Kruse N, Fang Q, et al. Experimental Results of a 10/40 kW-Class Reversible Solid Oxide Cell Demonstration System at Forschungszentrum Jülich. Journal of The Electrochemical Society 2023;170(4).
[18] Saarinen V. Experimental campaign results at system level.
[19] Saarinen V, Pennanen J, Kotisaari M, Thomann O, Himanen O, Iorio SD, et al. Design, manufacturing, and operation of movable 2 × 10 kW size rSOC system. Fuel Cells 2021;21(5):477–487.
[20] Mougin J, Aicart J, Gajewski A, Agrawal AK, Bergman H, Olivier P. Design, laboratory characterization, factory acceptance tests and installation of a 2.6 MW High temperature steam electrolyser in a refinery. International Journal of Hydrogen Energy 2025;141:1165–1171.
[21] Energy B. Bloom Energy Demonstrates Hydrogen Production with the World's Most Efficient Electrolyzer and Largest Solid Oxide System 2023 [Available from: https://www.bloomenergy.com/news/bloom-energy-demonstrates-hydrogen-production-with-the-worlds-most-efficient-electrolyzer-and-largest-solid-oxide-system/.
[22] Hajjaji N, Pons M-N, Houas A, Renaudin V. Exergy analysis: An efficient tool for understanding and improving hydrogen production via the steam methane reforming process. Energy Policy 2012;42:392–399.
[23] Ni M, Leung MK, Leung DY. Energy and exergy analysis of hydrogen production by solid oxide steam electrolyzer plant. International journal of hydrogen energy 2007;32(18):4648–4660.
[24] Müller R, Tsatsaronis G. Process integration and exergy-based assessment of high-temperature solid oxide electrolysis configurations. Energy Conversion and Management 2025;346:120106.
[25] Tsatsaronis G. Definitions and nomenclature in exergy analysis and exergoeconomics. Energy 2007;32(4):249–253.
[26] Koo T, Kim YS, Lee YD, Yu S, Lee DK, Ahn KY. Exergetic evaluation of operation results of 5-kW-class SOFC-HCCI engine hybrid power generation system. Applied Energy 2021;295:117037.
[27] Bui T, Lee D, Ahn KY, Kim YS. Techno-economic analysis of high-power solid oxide electrolysis cell system. Energy Conversion and Management 2023;278.
[28] TECHNOLOGIES SS. EBSILON®Professional 2018. Available at: <https://www.steag-systemtechnologies.com/en/products/ebsilon-professional/>. [accessed 13.2.2019].
[29] Bejan A, Tsatsaronis G, Moran MJ. Thermal Design and Optimization: Wiley; 1995.
[30] G. Goodwin D, K. Moffat H, Schoegl I, L. Speth R, W. Weber B. Cantera: An object-oriented software toolkit for chemical kinetics, thermodynamics, and transport processes. https://www.cantera.org, 2025. Version 3.2.0. 2025.
[31] Szargut J, Morris DR, Steward FR. Energy analysis of thermal, chemical, and metallurgical processes. United States: Hemisphere Publishing,New York, NY; None; 1987.
[32] Morris DR, Szargut J. Standard chemical exergy of some elements and compounds on the planet earth. Energy 1986;11(8):733–755.
[33] Siefert NS, Litster S. Exergy and economic analyses of advanced IGCC–CCS and IGFC–CCS power plants. Applied energy 2013;107:315–328.
[34] Wang F, Wang L, Ou Y, Lei X, Yuan J, Liu X, et al. Thermodynamic analysis of solid oxide electrolyzer integration with engine waste heat recovery for hydrogen production. Case Studies in Thermal Engineering 2021;27:101240.
[35] Choi S, Hong J. Versatile thermodynamic design of a solid oxide electrolysis cell system and its sensitivity to operating conditions. Energy Conversion and Management 2023;298:117776.
[36] García–García I, Izquierdo U, Barrio VL, Arias PL, Cambra JF. Power-to-Gas: Storing surplus electrical energy. Study of Al2O3 support modification. International Journal of Hydrogen Energy 2016;41(43):19587–19594.